



Supported by



Accepted Article

Title: One-pot synthesis of Cu/SAPO-34 with hierarchical pore using cupric citrate as a copper source for excellent NH₃-SCR of NO performance

Authors: Peiqiang Wang, Zhibin Li, Xiaotong Wang, Yongming Tong, Fulong Yuan, and Yujun Zhu

This manuscript has been accepted after peer review and appears as an Accepted Article online prior to editing, proofing, and formal publication of the final Version of Record (VoR). This work is currently citable by using the Digital Object Identifier (DOI) given below. The VoR will be published online in Early View as soon as possible and may be different to this Accepted Article as a result of editing. Readers should obtain the VoR from the journal website shown below when it is published to ensure accuracy of information. The authors are responsible for the content of this Accepted Article.

To be cited as: *ChemCatChem* 10.1002/cctc.202000818

Link to VoR: <https://doi.org/10.1002/cctc.202000818>

One-pot synthesis of Cu/SAPO-34 with hierarchical pore using cupric citrate as a copper source for excellent NH₃-SCR of NO performance

Peiqiang Wang[†], Zhibin Li[†], Xiaotong Wang, Yongming Tong, Fulong Yuan*, Yujun Zhu*

[†] Both authors contributed equally to this work

Mr. P Wang, Dr. Z Li, Ms. X Wang, Mr. Y Tong, Prof. F Yuan (Email: yuanfulong@hlju.edu.cn), Prof. Y Zhu (Email: yujunzhu@hlju.edu.cn)
Key Laboratory of Functional Inorganic Material Chemistry (Heilongjiang University), Ministry of Education, School of Chemistry and Materials, Heilongjiang University, Harbin 150080, PR China

Supporting information for this article is given via a link at the end of the document.

Abstract: It is still a serious challenge to develop a simple synthesized method of SAPO-34 sieve modified by Cu with high NH₃-SCR performance. The Cu/SAPO-34 samples with hierarchical structure were synthesized for the first time using cupric citrate as copper source by one-pot hydrothermal method which showed excellent NH₃-SCR performance for NO removal. Among them, the 0.15Cu/SAPO-34 catalyst with a Cu/Al ratio of 0.15 exhibited the widest temperature operating window (160-500 °C) and better hydrothermal stability. The physicochemical properties of 0.15Cu/SAPO-34 was measured to understand the impacts of the Cu species on the NH₃-SCR of NO activity by various characterization methods including XRD, NH₃-TPD, N₂ adsorption-desorption, XPS, EPR, UV-vis, NH₃-oxidation, NMR and *in situ* DRIFTS. The results reveal that the good activity is assigned to the isolated Cu species located at the site (I) in SAPO-34, and the co-existence of surface Cu²⁺ and Cu⁺ species with almost equal amounts. In addition, 0.15Cu/SAPO-34 also possesses suitable acidic sites which are conducive to catalytic activity. The results of *in situ* DRIFTS suggest that the NH₃-SCR reaction follows Eley-Rideal mechanism over 0.15Cu/SAPO-34.

Introduction

Nitrogen oxide (NO_x) is one of the major pollutants in air pollution, which is a problem that human beings need to solve urgently. Not only can NO_x cause a variety of environmental problems such as photochemical smog, but it can also pose human health to a huge threat.^[1] Currently, the selective catalytic reduction of NO_x with ammonia (NH₃-SCR) is considered to be the most effective method to convert NO_x into N₂ and H₂O.^[2] The catalysts suitable for NH₃-SCR reaction can be roughly divided into three types: noble metal, metal oxides and zeolite.^[3] By contrast, as a porous material with a large surface area, rich acidic sites and excellent shape-selective ability, zeolite is found to be more suitable for NH₃-SCR reaction.^[4] In the recent few years, transition metal and noble metal (Cu, Fe, Ce, Mn, Ag, Pt)-modified zeolites (ZSM-5, Beta, LTA),^[5] especially Cu modified small-pore zeolites (SAPO-34, SSZ-13),^[6] have become more and more popular research topics. Compared with other catalysts, copper modified SAPO-34, SSZ-13 exhibit wider activity temperature window, excellent N₂ selectivity, more outstanding hydrothermal stability, and superior H₂O and SO₂ resistance. Normally, the synthesis process of metal-exchanged zeolite involves multiple steps, which needs to

go through hydrothermal, washing, calcination, ammonia exchange, metal exchange, calcination and multiple drying in order.^[7] Additionally, the repeated ion exchange processes, drying and calcination processes increase significantly the complexity of the synthesis process. Ren et al. creatively used the inexpensive Cu-tetraethylenepentamine (Cu-TEPA) as the organic structure-directing agent (OSDA) instead of the expensive N,N,N-trimethyladamant ammonium hydroxide (TMAdaOH) by one step method to synthesize the Cu/SSZ-13 zeolite with good NH₃-SCR activity.^[8] However, the shortcomings of this method, such as high copper content and low hydrothermal stability, limit its further application.^[9] The catalytic performance and hydrothermal stability were improved by optimizing the synthesis method, adjusting the Si/Al ratio, and using the "reverse" ion exchange method to post-process the catalyst.^[10] Soon after the one-step method for synthesizing Cu/SSZ-13 with Cu-TEPA as the OSDA was proposed, and Corma's group applied this method to synthesize Cu/SAPO-34.^[6b,7] However, the NO conversion over the obtained Cu/SAPO-34 was low, which may be caused by the existence of a great quantity extra-framework copper species. To solve this problem, the synthesis strategy was optimized, and another template agent besides TEPA was introduced, and by adjusting the ratio of the two template agents, the copper loading can be precisely controlled.^[11] After hydrothermal treatment at 750 °C, the catalysts retained most of their original catalytic performance in the same temperature operating window of 250-450 °C. In order to further increase mass transfer and shorten the reactant transport path, the hierarchical pore structure was introduced into the zeolite catalyst.^[12] Liu et al. prepared a kind of Cu/SAPO-34 with meso-microporous with Cu-TEPA and DIEPA as the co-OSDA by the one-pot route, the synthesized Cu/SAPO-34 showed an excellent NH₃-SCR performance in the operating temperature window of 150-425 °C, but the hydrothermal stability was not discussed.^[13] In addition to Cu-TEPA, there are many copper complexes suitable for one-step method as the copper source, but some conditions need to be met, for example, the complex molecule is easily available, the size of the complex molecule cannot exceed the size of the CHA cage,^[8] and need stably exist in the synthetic sol, etc. In general, it is still a serious challenge to develop a simple synthesized method of Cu modified SAPO-34 with good NH₃-SCR performance, high hydrothermal stability and resistance of SO₂. In this paper, a series of Cu/SAPO-34 with different Cu/Al ratios were successfully synthesized firstly by using hard template method and controlling the different Cu/Al ratios. It was noticed

that the catalysts exhibit good NH₃-SCR performance, but only 0.15Cu/SAPO-34 with the Cu/Al ratio of 0.15 shows the CHA structure of SAPO-34 according to the XRD results. Moreover, 0.15Cu/SAPO-34 was also observed superior hydrothermal stability and resistance to SO₂ and H₂O.

Results and Discussion

In this work, a series of hierarchical xCu/SAPO-34 which was obtained by using different ratios of Cu/Al ($x=0.05, 0.10, 0.15, 0.20$) was synthesized by facile one-pot hydrothermal process. The XRD patterns (Figure S1) reveal that only 0.15Cu/SAPO-34 with the Cu/Al ratio of 0.15 shows the pure CHA topology and other samples present the mixed phases of SAPO-34 and SAPO-5, moreover, the 0.15Cu/SAPO-34 catalyst also exhibits the best NH₃-SCR of NO performance (Figure S2). Therefore, the relationship between structure and activity over 0.15Cu/SAPO-34 was studied in detail through following various characterization and activity tests.

The NO conversion is given in Figure 1A over 0.15Cu/SAPO-34 under different gas hourly space velocity (GHSV). An obvious decline in the NO conversion is observed with the increase in GHSV when the temperature of the NH₃-SCR reaction is below 200 °C. The activity temperature window (>90% NO conversion) can be maintained in the range of 180-500 °C under the GHSV of 80,000 h⁻¹. Moreover, the NO conversion only exhibits slight decrease at high temperature when the GHSV is increased to 120,000 h⁻¹. It is interesting that the operating temperature window can still be maintained in the range of 200-450 °C when the GHSV reaches 240,000 h⁻¹. According to above results, it can be summarized that the NO conversion decreases slightly with the increase of GHSV at low and high temperature, indicating the excellent NH₃-SCR performance over 0.15Cu/SAPO-34 even at higher GHSV condition. The activity of catalyst prepared by ion-exchange method is also provided to distinguish the difference between the two methods and the result is shown in Figure (S3). Under the GHSV is 40000 h⁻¹, the catalyst prepared by one-pot method shows comparable catalytic performance to the catalyst prepared by ion-exchange method.

In order to simulate the realistic NH₃-SCR reaction condition,^[14] the effects of H₂O or/and SO₂ on the activity were tested. Figure 1B shows the H₂O or/and SO₂ resistance over the 0.15Cu/SAPO-34 at 200 °C under the GHSV of 40,000 h⁻¹. In the beginning, the activity remains stable for about 4 h in the absence of H₂O and SO₂. After that, 5% H₂O is added into the feed, it is clear seen that NO conversion still maintains at 100%. After 8 h, 100 ppm of SO₂ is injected into the reactor, NO conversion is observed to be a slight decrease. While the H₂O and SO₂ are cut off, the NO conversion restores to 100% rapidly. It is interesting that the 0.15Cu/SAPO-34 catalyst can still maintain excellent catalytic performance in the presence of 10% H₂O. While the NO conversion reduces to 95% with the SO₂ concentration increases to 200 ppm. Although the NO conversion cannot restore completely after cutting off H₂O and SO₂, it can still be maintained at about 98%. These results demonstrate that the 0.15Cu/SAPO-34 exhibits superior NH₃-SCR performance on resistance of H₂O and SO₂.

The presence of water vapor in the environment is unavoidable.^[15] It is necessary to investigate the influence of the

hydrothermal aging of the catalyst on activity. The 0.15Cu/SAPO-34 was hydrothermal treated at low temperature (80 °C, 10% H₂O, 48 h) and high temperature (700 °C, 10% H₂O, 12 h), respectively. As exhibited in Figure 1C, the NO conversion shows obvious decrease in low temperature region of 100-180 °C over the 0.15Cu/SAPO-34 treated at low temperature, and the activity window becomes slightly narrow (175-475 °C) compared with the fresh catalyst. More interestingly, as demonstrated in Figure 1D, the 0.15Cu/SAPO-34 catalyst treated at high temperature displays the similar catalytic performance to the treatment at low temperature. These results suggest that the 0.15Cu/SAPO-34 can exhibit superior hydrothermal stability. The deactivation of Cu/SAPO-34 after hydrothermal treatment can be attributed to two aspects. One is the destruction of the CHA structure is derived from the hydrolysis of the Si-O-Al bonds in the zeolite framework. And another is the migration and polymerization of active Cu species. While isolated Cu²⁺ is considered to be the main active species for NH₃-SCR reaction, and a large number of Cu²⁺ species are more likely to polymerize during hydrothermal treatment. However, some researchers found that the presence of moderate amount of Cu⁺ can promote the low temperature NH₃-SCR reaction, attributed to enhancing the redox cycle between Cu²⁺ and Cu⁺.^[16] In this work, the ratio of Cu²⁺/Cu⁺ calculated by the XPS results below is 1.2 in the 0.15Cu/SAPO-34. This higher Cu⁺/(Cu²⁺ + Cu⁺) ratio is favor of both the good SCR activity and the possibility for the excellent hydrothermal stability.

In short, using CaCO₃ as the hard template and cupric citrate as the copper source, we have successfully prepared a NH₃-SCR deNO_x catalyst with high NO conversion, excellent hydrothermal stability and tolerance of H₂O and SO₂.

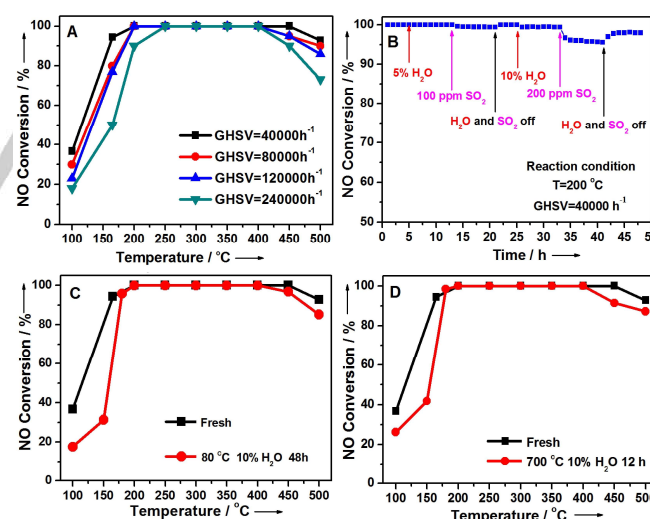


Figure 1. NH₃-SCR activity under different conditions of GHSV (A), SO₂ and H₂O (B) and hydrothermal aging at low (C) and high (D) temperature over 0.15Cu/SAPO-34.

Figure 2 shows the XRD patterns of pure SAPO-34 and 0.15Cu/SAPO-34. Obviously, both SAPO-34 and 0.15Cu/SAPO-34 present the diffraction peaks at 2θ of about 9.5, 14.0, 16.1, 17.8, 20.7, 25.0 and 30.7 °, belonging to the CHA topological structure,^[12] which indicates that the introduction of Cu ions has no effect on the formation of CHA topological structure for

0.15Cu/SAPO-34. However, the crystallinity of 0.15Cu/SAPO-34 is observed an obvious decrease compared with the SAPO-34. Moreover, the diffraction peaks for 0.15Cu/SAPO-34 shift to low angle compared with pure SAPO-34 slightly. The above phenomena may be due to the crystal distortion caused by the introduction of Cu ions. In addition, no obvious diffraction peaks of CaCO_3 and CuO are observed from the XRD spectrum,^[17] which suggests that the CaCO_3 should be removed thoroughly and the content of the CuO_x species is very low or highly dispersed in SAPO-34 evenly.

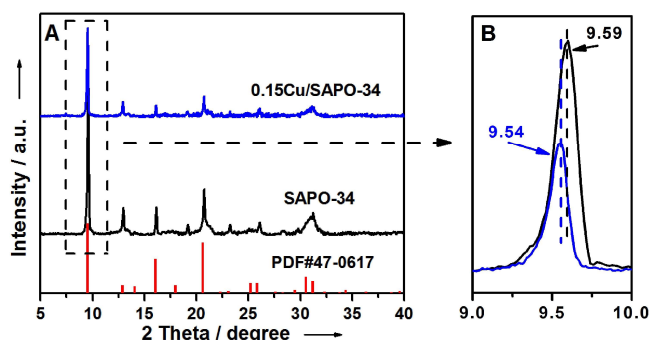


Figure 2. XRD patterns of SAPO-34 (black) and 0.15 Cu/SAPO-34 (blue).

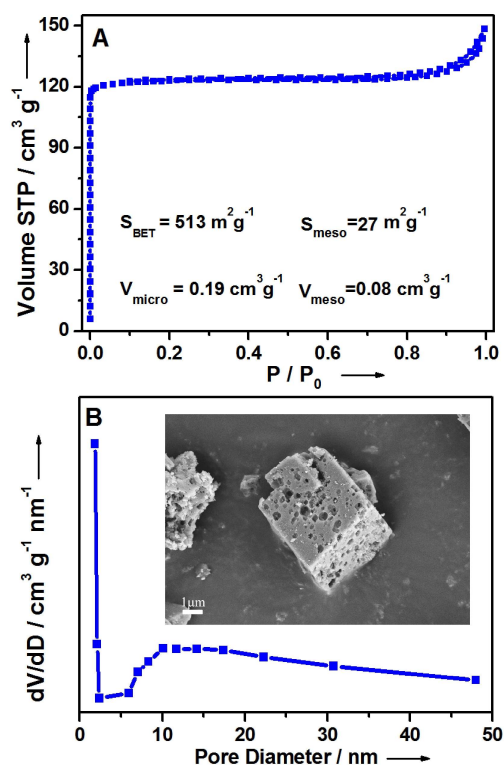


Figure 3. N_2 adsorption-desorption isotherms (A) and the pore diameter distribution and the SEM image (B) of 0.15Cu/SAPO-34.

The N_2 adsorption-desorption isotherms, pore diameter distribution and SEM image of 0.15Cu/SAPO-34 are shown in Figure 3. As can be seen from Figure 3A, the N_2 adsorption amount increases rapidly at low relative pressure ($P/P_0 < 0.1$)

and a hysteresis loop can be observed at high relative pressure ($0.6 < P/P_0 < 0.9$). As listed in Figure 3A, the BET surface area (S_{BET}) of 0.15Cu/SAPO-34 is calculated to $513 \text{ m}^2\cdot\text{g}^{-1}$, the surface area of mesopores is $27 \text{ m}^2\cdot\text{g}^{-1}$, while the micropores volume (V_{micro}) and mesopores volume (V_{meso}) calculated are $0.19 \text{ cm}^3\cdot\text{g}^{-1}$ and $0.08 \text{ cm}^3\cdot\text{g}^{-1}$, respectively. The results of N_2 adsorption-desorption measurements demonstrate that micropores and mesopores coexist in the 0.15Cu/SAPO-34 sample. Many mesopores with the pore diameter of about 6-30 nm can be observed from the result of BJH pore diameter distribution besides the existence of micropores. The SEM image of 0.15Cu/SAPO-34 also confirms the results displayed in inserted Figure 3B. It can be observed that the 0.15Cu/SAPO-34 exhibits the cubic morphology with many mesopores created by the elimination of CaCO_3 . Thus, the above consequences reveal that the 0.15Cu/SAPO-34 sample possesses hierarchical pores structure.

The N_2 adsorption-desorption isotherms, pore diameter distribution and SEM image of 0.15Cu/SAPO-34 are shown in Figure 3. As can be seen from Figure 3A, the N_2 adsorption amount increases rapidly at low relative pressure ($P/P_0 < 0.1$) and a hysteresis loop can be observed at high relative pressure ($0.6 < P/P_0 < 0.9$). As listed in Figure 3A, the BET surface area (S_{BET}) of 0.15Cu/SAPO-34 is calculated to $513 \text{ m}^2\cdot\text{g}^{-1}$, the surface area of mesopores is $27 \text{ m}^2\cdot\text{g}^{-1}$, while the micropores volume (V_{micro}) and mesopores volume (V_{meso}) calculated are $0.19 \text{ cm}^3\cdot\text{g}^{-1}$ and $0.08 \text{ cm}^3\cdot\text{g}^{-1}$, respectively. The results of N_2 adsorption-desorption measurements demonstrate that micropores and mesopores coexist in the 0.15Cu/SAPO-34 sample. Many mesopores with the pore diameter of about 6-30 nm can be observed from the result of BJH pore diameter distribution besides the existence of micropores. The SEM image of 0.15Cu/SAPO-34 also confirms the results displayed in inserted Figure 3B. It can be observed that the 0.15Cu/SAPO-34 exhibits the cubic morphology with many mesopores created by the elimination of CaCO_3 . Thus, the above consequences reveal that the 0.15Cu/SAPO-34 sample possesses hierarchical pores structure.

The valence states of different copper species on the catalyst surface are monitored with XPS and the results are shown in Figure 4A. The $\text{Cu}2\text{p}$ spectrum can be deconvoluted into five peaks. According to literatures,^[18] the two peaks belonging to $\text{Cu}2\text{p}_{3/2}$ is assigned to Cu^+ species at binding energy (BE) of 933 eV and Cu^{2+} species at BE of 935.4 eV. The satellite peak is 10 eV higher than the $\text{Cu}2\text{p}_{3/2}$ peak, which is the essential characteristic of the Cu^{2+} species. The peak of $\text{Cu}2\text{p}_{1/2}$ at the high BE can be fitted into two peaks by deconvolution. The peak at 952.8 eV is assigned to Cu^+ , while the peak at 955.4 eV is ascribed to Cu^{2+} . The peaks at high BE of 935.4 and 955.4 eV correspond to the isolated Cu^{2+} species coordinated to the framework oxygen atoms of SAPO-34 zeolite, while the peaks at 933 and 952.8 eV are ascribed to the isolated Cu^+ species.^[6a, 19] The $\text{Cu}^{2+}/\text{Cu}^+$ ratio is analyzed in terms of Gaussian deconvolution based on the peak area, and it is 1.2 for the 0.15Cu/SAPO-34 catalyst. The XPS results present that the 0.15Cu/SAPO-34 catalyst possesses a moderate Cu^{2+} content (4.1%) and a suitable content of Cu^+ , which is in favor of the redox cycle of copper species during the NH_3 -SCR process. Schneider et al.^[20] confirmed that Cu^+ and Cu^{2+} are propitious to NH_3 -SCR reaction by XAFS and DFT calculation, the NO and O_2 are more inclined to adsorbed on Cu^+ , at the same time Cu^+ is

oxidized to Cu^{2+} , while the Cu^{2+} can be deoxidized to Cu^+ after NH_3 is adsorbed.

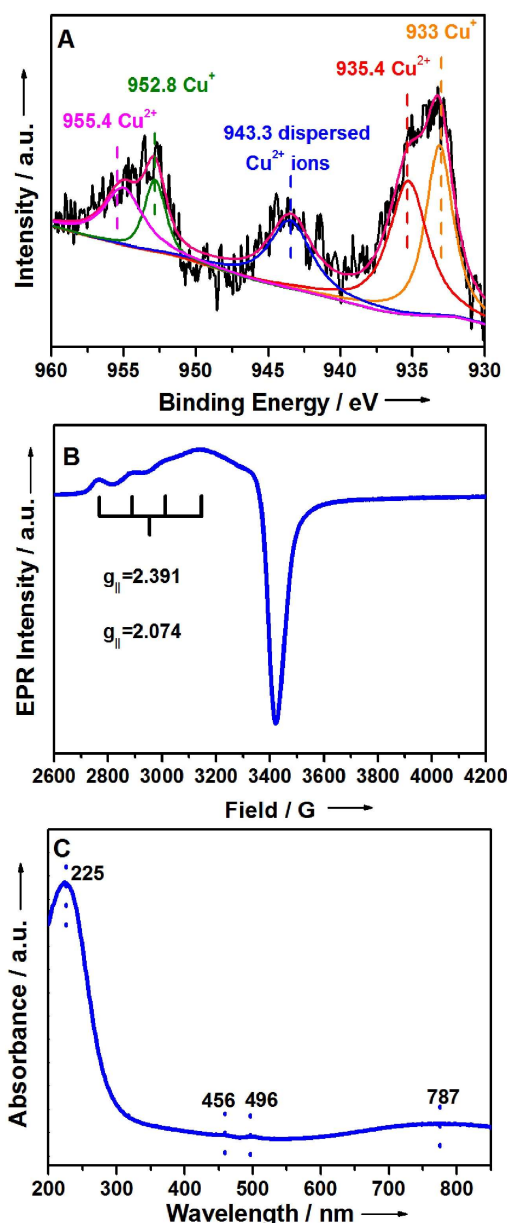


Figure 4. Cu 2p XPS (A), EPR spectrum (B) and UV-vis curve (C) of 0.15Cu/SAPO-34.

EPR spectrum is an efficient technology to discriminate the location environment of Cu^{2+} in the catalyst. For all the Cu species, like Cu^{2+} , Cu^+ and CuO etc., only the isolated Cu^{2+} species can produce EPR signals, and other Cu species is silent. Cu^{2+} species can be located at four sites in Cu/SAPO-34 framework and the Cu^{2+} species in different sites shows various EPR parameters. As displayed in Figure 4B, the EPR signal exhibits at $g_{||}$ (2.388) and $A_{||}$ (125 G) for 0.15Cu/SAPO-34, which indicates that all Cu^{2+} species exists in the same coordination environment (Site I), located at the junction of the D6R and the CHA cage in the catalyst.^[5c,6a] According to literature,^[21] hyperfine splitting coincident with the interaction of unpaired

electrons, and the value of $g_{||}$ (2.388) corresponds the isolated Cu^{2+} species with axial symmetry. Zamadics et al.^[22] discovered that the EPR signal was accordant with the isolated Cu^{2+} ions octahedrally coordinated to three framework oxygen atoms and three water molecules which located in Site (I). Normally, the Site (I) is regarded as the easier approachable site to the adsorbates (NH_3 and NO) than others. The isolated Cu^{2+} species located this position may be main reason leading to the excellent NH_3 -SCR performance of the 0.15Cu/SAPO-34.

For understanding the Cu species and its coordination nature in SAPO-34, UV-vis spectrum was tested for 0.15Cu/SAPO-34 (Figure 4C). Two obvious bands (225 and 787 nm) and two weak bands (456 and 496 nm) can be observed from the UV-vis spectrum. As reported in the literatures,^[23] the band at 225 nm can be attributed to the charge transition between O of SAPO-34 and $\text{Cu}^+/\text{Cu}^{2+}$, while the signal of CuO particles can be found in the broad band at about 787 nm which is ascribed to the electron d-d transitions of Cu^{2+} in distorted octahedral surrounding by oxygen. The signal of the charge transition bands of O-Cu-O and Cu-O-Cu complexes can be found at 457 and 499 nm,^[24] respectively. These bands confirm that Cu^{2+} , Cu^+ and CuO co-exist in 0.15Cu/SAPO-34 again.

The amount and strength of acid sites are two essential elements for NH_3 -SCR catalysts. In order to understand the relationship between acidity and activity, NH_3 -TPD was measured over SAPO-34 and 0.15Cu/SAPO-34. For 0.5Cu/SAPO-34, the peaks at different temperature are assigned to the NH_3 desorption on the acid sites of different strength according to literatures.^[6c,25] The strong peak at 150 °C and the shoulder peak at 250 °C represent the adsorbed NH_3 molecules on weak Brønsted acid sites of SAPO-34 and weak Lewis acid sites related to Cu species. The peak at 450 °C is ascribed to the residual structural Brønsted acid sites of SAPO-34 and moderate Lewis acid sites related to Cu species. The peak at 510 °C stands for the adsorbed NH_3 molecules on both strong Brønsted acid sites of SAPO-34 and new Lewis acid sites created by Cu species. For SAPO-34, the ascription of the peaks at 150 and 250 °C are similar with 0.15Cu/SAPO-34. However, the peak at 480 °C is much smaller compared with literatures.^[25c,d] The reason may be attributed to the different amount and pathway of Si atoms replacing Al atoms and P atoms in the formation of SAPO-34 derived from different materials, feeding sequence, template agents etc. The calculated total acid amounts are listed in Figure 5A. Compared with the SAPO-34, 0.15Cu/SAPO-34 exhibits fewer acid sites at low temperature but more amount acid sites at high temperature which may be the main reason contributed to its good NH_3 -SCR performance. The acidity on the catalyst surface is known to be the vital factor for the adsorption of NH_3 , which is closely related to the deNO_x performance. The appropriate amount and strength of acid sites are more conducive to the reaction, enhancing the catalytic performance to a certain degree. In addition, the NH_3 oxidation test was performed in order to study the oxidation capacity and the relationship between NH_3 conversion and reaction temperature over 0.15Cu/SAPO-34. As given in Figure 5B, the conversion of NH_3 is very low at low temperature below 250 °C, however, it increases rapidly above 250 °C and completely consumes at 450 °C. Combined with the activity (Figure 1A), it is suggested that the decrease in NO conversion at high temperature should be ascribed to the excessive oxidation of NH_3 .^[26]

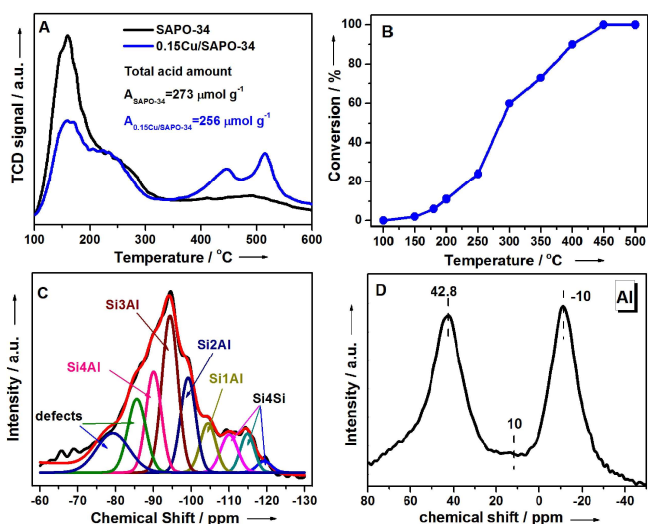


Figure 5. NH₃-TPD profile (A), NH₃ oxidation (B), ²⁹Si MAS NMR spectrum (C) and ²⁷Al MAS NMR spectrum (D) of 0.15Cu/SAPO-34.

Solid-state NMR spectra tests were used to comprehend the coordination type of Si and Al species in the zeolite framework. The ²⁹Si MAS NMR measurement result of 0.15Cu/SAPO-34 is shown in Figure 5C. Many kinds of Si species can be observed from the deconvolution results of ²⁹Si solid-state NMR spectrum. The peaks at -110, -104, -99, -95 and -91 ppm are assigned to the Si₄Si, Si₁Al₃Si, Si₂Al₂Si, Si₃Al₁Si and Si₄Al species, respectively. While the peaks at -80 and -86 ppm can be attributed the structure defects, and the peak at about -115 ppm belongs to the Si islands.^[27] The Si species percentage was calculated according to the deconvolution results listed in Table S1. By comparing the amount of different silicon species in 0.15Cu/SAPO-34 and SAPO-34, two conspicuous changes can be observed that the amount of the Si species defects increases and the content of the Si₄Al species decreases for 0.15Cu/SAPO-34. Due to the large radius of copper ion, the introduction of copper ion leads to the lattice distortion of 0.15Cu/SAPO-34, resulting in the formation of more defects. Meanwhile, the introduced Cu ion occupies a part of -OH can bring about the decrease in Si₄Al and acidity, which is consistent with the NH₃-TPD results. As displayed in Figure 5D and S4, for ²⁷Al MAS NMR spectra of the two samples, the signals at 42.8, 10 and -10 ppm are assigned to tetrahedral, pentahedral and octahedral coordinated Al atoms, respectively.^[6a,28] Interestingly, a large amount of octahedral coordinated Al atoms can be obtained in the samples, which indicates that a portion of Al may not be involved in the formation of the zeolite framework or dealumination occurs when removing CaCO₃ with HCl. Compared with SAPO-34, the amount of octahedral coordinated Al species in 0.15Cu/SAPO-34 increases a lot, which may be due to the fact that the addition of Cu ion leads to the change in the coordination mode and ability of the framework Al.^[29] By comparing the changes of Si and Al species between SAPO-34 and 0.15Cu/SAPO-34, it is found that the introduction of copper has a significant effect on the amount of strong and weak acid sites.

NH₃ adsorption was recorded at different time by in situ DRIFTS over 0.15Cu/SAPO-34 and the results are exhibited in Figure 6A. Several bands can be observed in the region of 1100-1300,

3240-3350, 3580-3700 cm⁻¹ after the 0.15Cu/SAPO-34 sample is exposed to NH₃ at 200 °C. Moreover, the intensity of those bands increases with the adsorption time. According to literatures,^[30] the bands at about 1188 and 1260 cm⁻¹ are assigned to asymmetric vibration of N-H bands in NH₃ species adsorbed on the Lewis acid sites, and the bands at about 3245, 3280 and 3341 cm⁻¹ are ascribed to symmetric and asymmetric bending vibrations of the coordinated NH₄⁺. Meanwhile, two obvious negative bands at 3600 and 3617 cm⁻¹ can be attributed to NH₃ adsorbed on the bridged Al-(OH)-Si Brønsted acid sites, and their intensities progressively increase with time.^[23a] The above results of NH₃ adsorption illuminate that there are abundant Lewis acid sites and Brønsted acid sites on the surface of 0.15Cu/SAPO-34 catalyst. These acid sites provide the favorable conditions for NH₃ adsorption and activation which are more conducive to NH₃-SCR reaction.

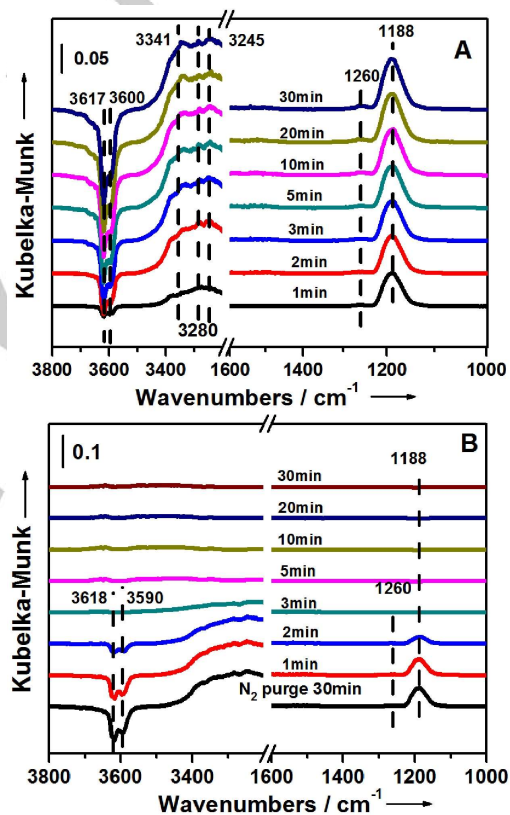


Figure 6. In situ DRIFTS of NH₃ adsorption (A) and reaction between NO+O₂ and pre-adsorbed NH₃ (B) on 0.15Cu/SAPO-34 at 200 °C.

The NO+O₂ were introduced into the system after the NH₃ adsorption purged by N₂ for 30 min to investigate the reaction between pre-adsorbed NH₃ and the NO+O₂. As shown in Figure 6B, the intensities of all the NH₃ adsorption bands only exhibit a slightly reduction after purged by N₂. When NO+O₂ is injected, the peaks of all ammonia species decrease sharply. Only 3 minutes later, almost all the peaks belong to the NH₃ adsorption disappear, which reveals that whether the NH₃ adsorbed on the Brønsted or Lewis acid sites can participate the reaction with gaseous NO + O₂ immediately.

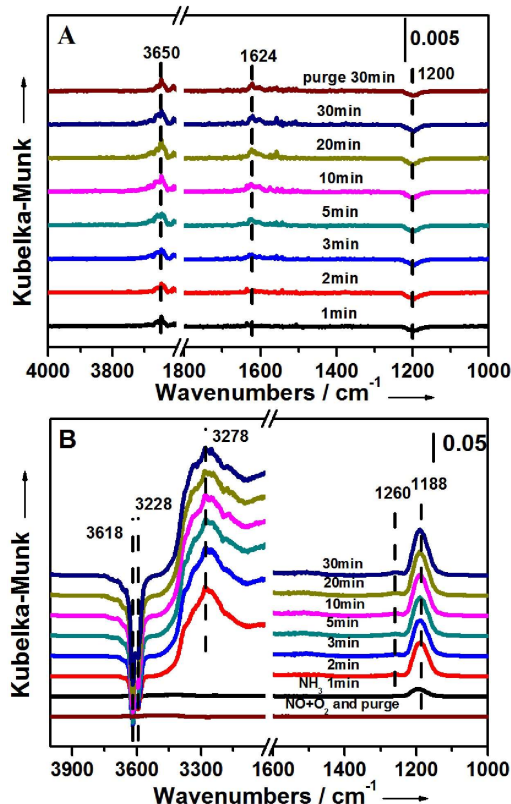


Figure 7. *In situ* DRIFTS of NO adsorption (A) and reaction between NH_3 and pre-adsorbed $\text{NO}+\text{O}_2$ (B) on 0.15Cu/SAPO-34 at 200 °C.

To research the adsorption of $\text{NO}+\text{O}_2$ at different time over 0.15Cu/SAPO-34, the *in situ* DRIFTS tests were carried on. As displayed in Figure 7A, $\text{NO}+\text{O}_2$ adsorbed on the surface of 0.15Cu/SAPO-34 can engender many kinds of nitrate species, such as monodentate nitrate, bridged nitrate, bidentate nitrate, etc.^[18a] The negative band at 1200 cm^{-1} can be assigned to nitrite which is generated by $\text{NO} + \text{O}_2$ adsorbed on the surface of 0.15Cu/SAPO-34.^[12] While the bands between 1500 and 1700 cm^{-1} are quite complicated, most of the bands cannot stable existence on the catalyst surface. But the intensity of the band at 1624 cm^{-1} increases with the extension of contact time with $\text{NO}+\text{O}_2$, belonging to the adsorbed NO_2 species formed by the reaction NO and O_2 .^[31] On the whole, it is not easy for NO_x to absorb on the 0.15Cu/SAPO-34 catalyst. Even if the signals are amplified 10 times, the intensities of all these bands are too weak to discern easily. The results of the reaction between pre-adsorbed $\text{NO}+\text{O}_2$ and NH_3 are shown in Figure 7B. As NH_3 is introduced, the adsorbed NO_x species disappears and the characteristic peaks of adsorbed NH_3 species appear immediately. We can draw a conclusion that the generation of NO_2 can promote the “Fast SCR” reaction to some extent although the amount of pre-adsorbed $\text{NO}+\text{O}_2$ on the catalyst surface is far fewer.^[32]

To sum up, whether it is pre-adsorbed NH_3 or $\text{NO}+\text{O}_2$, the reaction rate occurs on 0.15Cu/SAPO-34 is very rapid. Base on the much weaker NO_x adsorption and massive adsorbed NH_3 species, we think that the NH_3 -SCR reaction may mainly follow the Eley-Rideal (E-R) mechanism over 0.15Cu/SAPO-34.

Conclusion

By using cupric citrate as the copper source, TEA as the organic structure-directing agent, and CaCO_3 as the hard template to build mesopore, we have successfully synthesized copper modified SAPO-34 zeolite (0.15Cu/SAPO-34) with micro-mesoporous hierarchical pore by facile one-step hydrothermal method. 0.15Cu/SAPO-34 shows the superior NH_3 -SCR performance for NO removal with the wide activity temperature window of 165–500 °C, even after hydrothermal treatment with 10% H_2O at low (80 °C) or high (700 °C) temperature. Moreover, the catalyst also shows good NH_3 -SCR activity under high GHSV and noticeable resistance to H_2O and SO_2 . Combined the XPS results, the suitable Cu^+ and Cu^{2+} species on the catalyst is closely related to the NH_3 -SCR activity. In addition, we propose that the NH_3 -SCR of NO mainly follows the E-R mechanism over 0.15Cu/SAPO-34. Compared with our previous work, this method can reduce the time required for synthesis while maintaining the wide activity temperature window. In summary, this is an efficient and economic method to synthesize the Cu/SAPO-34 with excellent deNO_x performance.

Experimental Section

$x\text{Cu}/\text{SAPO-34}$ ($x=0.05, 0.10, 0.15, 0.20$) zeolites with hierarchical pore in which x represents the theoretical Cu/Al ratio, were prepared by one-pot hydrothermal synthesis method with cupric citrate and CaCO_3 as the copper source and hard template, respectively. The synthesis steps of $x\text{Cu}/\text{SAPO-34}$ are as follows: (1) 3.55 g pseudoboehmite (71 wt% Al_2O_3 , Kermel Company) and 30 mL distilled water were added into beakers and stirred at room temperature. (2) After 2 h, 3.25 mL H_3PO_4 (85 wt%, Kermel company) was added to the solution and stirred 2–3 h. (3) 1.5 g of SiO_2 as the silicon source was introduced into the mixture under stirring and continually stirred for 2 h. (4) 7.5 mL triethylamine (TEA) as the OSDA was slowly introduced into the solution for 2 h. (5) With the Cu/Al ratios were set as 0.05, 0.10, 0.15 and 0.20, cupric citrate as the copper source was put into the gel and then stirred overnight. (6) In the interest of producing the hierarchical pore in the catalysts, 2 g CaCO_3 was introduced into the mixture and 5 mL distilled water and 5 mL ethanol were injected to promote the dispersion of CaCO_3 . (7) The final solution was transferred into 50 mL autoclaves and heated at 200 °C for 48 h. Then the product was washed by water to remove the raw material and 0.2 mol/L HCl solution was used to remove the CaCO_3 . (8) The catalysts were dried at 100 °C to remove the water and calcined at 600 °C for 5 h to remove OSDA. SAPO-34 was also synthesized according to the above description except without adding cupric citrate.

The powder X-ray diffraction (XRD) patterns were measured from 5–50 ° on Bruker D8 Advance X-ray diffract meter system in the radiation of Cu $\text{K}\alpha$ ($\lambda=0.15418$ nm) at 40 mA and the step size of 0.02 °·s⁻¹. Scanning electron microscope (SEM) images were measured on a Hitachi S-4800 microscope at 20 kV. BET surface area and pore characterization were measured on Micromeritics ASAP 2020 Plus by N_2 adsorption-desorption at the temperature of -196 °C. Before testing, the sample (0.100 g) was pretreated in the vacuum condition with heating at 200 °C for 5 h. The amount of Cu was obtained on inductive coupled plasma optical emission spectrometer (ICP-OES) (NexION 350D). The X-ray photoelectron spectroscopy (XPS) was performed by the Kratos-Axis ULTRA DLD with the Al $\text{K}\alpha$ radiation source. The binding energy (BE) was referred through the C 1s (BE = 284.6 eV). The electron paramagnetic resonance (EPR) spectrum was measured on the Bruker EPR A200 instrument.

²⁷Al and ²⁹Si nuclear magnetic resonance (NMR) measurements were carried on the Bruker Avance III 400 spectrometer. ²⁷Al chemical shift and ²⁹Si chemical shift were referred to Al(NO₃)₃ of 1 mol/L and Kaolin, respectively. And the ²⁷Al NMR and ²⁹Si NMR data were recorded with a spinning rate of 12 kHz and 6 kHz, respectively. Temperature programmed desorption of ammonia (NH₃-TPD) curves were monitored on TP5080 (Tianjin XQ) with TCD. The catalyst (0.100g) was transferred into the tube, pre-treated at 300 °C with He to remove the physically adsorbed water and other gases on the catalysts. And then it cooled down to 100 °C to adsorb NH₃ for 30 min. Finally, the temperature was increased from 100 °C to 700 °C at a rate of 10 °C /min to record the desorption curve.

In situ diffuse reflection infrared Fourier transform spectroscopies (DRIFTS) were measured on Thermo Nicolet 6700 with MCT detector cooled by the liquid N₂. At the first, the catalyst was placed into the IR cell (Harrick) meanwhile the temperature was increased to 300 °C and kept for 1 h with N₂ sweeping. After that the temperature was maintained at 200 °C to collect the background. All the data were recorded by collecting 32 scans at 4 cm⁻¹ resolution in the whole test regions (650-4000 cm⁻¹). The test conditions were as follows: 1000 ppm NO, 1000 ppm NH₃, 3% O₂, N₂ as balance gas, and the total flow rate was kept at 200 mL min⁻¹.

NH₃-SCR performances were measured on the fixed-bed quartz tubular flow reactor. The reaction gas consists of 1000 ppm NO, 1000 ppm NH₃, 5% O₂, 10% H₂O (if used) and N₂ as the balance. The total gas flow rate was controlled at 200 mL min⁻¹, which is equivalent to a gas hourly space velocity (GHSV) of 40,000 h⁻¹. The concentrations of the outlet gas were monitored by Nicolet 6700 which was equipped with a gas cell (PIKE, 2.4 m). At each testing temperature, the reaction was stable for at least 30 min before collecting data. To investigate the effect of hydrothermal treatment on activity, the catalyst was also treated at high temperature (700 °C, 12 h) and low temperature (80 °C, 24 h) in the fixed-bed reactor in the presence of water vapor was 10%, respectively. After the treatment, the catalyst was heated at 600 °C under N₂ to eliminate the adsorbed H₂O. The conversion of NO and the selectivity of N₂ were calculated by the expressions (1) and (2):

$$\text{NO conversion} = \frac{[\text{NO}]_{\text{in}} - [\text{NO}]_{\text{out}}}{[\text{NO}]_{\text{in}}} \times 100\% \quad (1)$$

$$\text{N}_2 \text{ selectivity} = \left(1 - \frac{[\text{NO}_2]_{\text{out}} + 2 \times [\text{N}_2\text{O}]_{\text{out}}}{[\text{NO}]_{\text{in}} + [\text{NH}_3]_{\text{in}} - [\text{NO}]_{\text{out}} - [\text{NH}_3]_{\text{out}}}\right) \times 100\% \quad (2)$$

The [NO]_{in} and [NH₃]_{in} represent the concentrations of inlet gas for NO and NH₃, respectively; while [NO]_{out}, [NH₃]_{out}, [N₂O]_{out} and [NO₂]_{out} denote the outlet gas concentrations of NO, NH₃, N₂O, NO₂, respectively.

The oxidations of NH₃ were measured on the fixed-bed quartz tubular flow reactor. The reaction gas consists of 1000 ppm NH₃, 5% O₂, and N₂ as the balance. The total gas flow rate was controlled at 200 mL min⁻¹; the concentrations of the outlet NH₃ were monitored by Nicolet 6700. The conversion of NH₃ was calculated by the expression (3)

$$\text{NH}_3 \text{ conversion} = \frac{[\text{NH}_3]_{\text{in}} - [\text{NH}_3]_{\text{out}}}{[\text{NH}_3]_{\text{in}}} \times 100\% \quad (3)$$

Acknowledgements

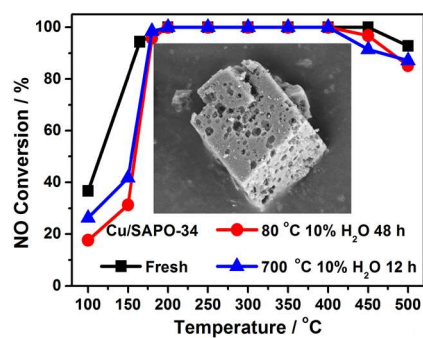
This work is supported by Harbin science and technology innovation talent fund (Outstanding academic leader project) (RC2016XK015004).

Keywords: one-pot hydrothermal method • Cu/SAPO-34 • selective catalytic reduction of NO with NH₃ • cupric citrate • high hydrothermal stability

- [1] a) M. Kampa, E. Castanas, *Environ. Pollution* **2008**, 151, 362-367. b) S. Lal, R.S. PATIL, *Environ. Monit. Assess.* **2001**, 68, 37-50. c) E. Anyanwu, *Environ. Health* **1999**, 14, 169-185.
- [2] H.T. Hug, A. Mayer, A. Hartenstein, *SAE Technol.* **1993**, 3, 1-5.
- [3] a) W. Held, A. König, T. Richter, L. Puppe, *J. Fuels & Lubr.* **1990**, 99, 209-216. b) K. Shimizu, A. Satsuma, T. Hattori, *Catal. Surv. Jpn.* **2000**, 4, 115-123. c) G. Busca, M.A. Larrubia, L. Arrighi, G. Ramis, *Catal. Today* **2005**, 108, 139-148.
- [4] a) Y. Li, L. Li, J.H. Yu, *Chem* **2017**, 3, 928-949. b) S.S.R. Putluru, A. Riisager, R. Fehrmann, *Appl. Catal. B* **2010**, 97, 333-339.
- [5] a) M. Iwamoto, H. Furukawa, Y. Mine, F. Uemura, S. Mikuriya, S. Kagawa, *Chem. Soc. Chem. Commun.* **1986**, 1272-1273. b) P.N.R. Vennestrøm, T.V.W. Janssens, A. Kustov, M. Grill, A. Puig-Molina, L.F. Lundegaard, R. Tiruvalam, P. Concepción, A. Corma, *J. Catal.* **2014**, 309, 477-490. c) L. Chen, X.X. Wang, Q.L. Cong, H.Y. Ma, S.J. Li, W. Li, *Chem. Eng. J.* **2019**, 369, 957-967. d) O. Mihai, C.R. Widyastuti, S. Andonova, K. Kamasamudram, J.H. Li, S.Y. Joshi, N.W. Currier, A. Yezerets, L. Olsson, *J. Catal.* **2014**, 311, 170-181. e) C. Peng, J. Liang, H.G. Peng, R. Yan, W.M. Liu, Z. Wang, P. Wu, X. Wang, *Ind. Eng. Chem. Res.* **2018**, 44, 14967-14976.
- [6] a) J. Wang, D.Q. Fan, T. Yu, J.Q. Wang, T. Hao, X.Q. Hu, M.Q. Shen, W. Li, *J. Catal.* **2015**, 322, 84-90. b) R. Martínez-Franco, M. Moliner, P. Concepción, J.R. Thogersen, A. Corma, *J. Catal.* **2014**, 314, 73-82. c) K.P. Xie, J.W. Woo, D. Bernin, A. Kumar, K. Kamasamudram, L. Olsson, *Appl. Catal. B* **2019**, 241, 205-216. d) A.M. Beale, I. Lezcano-Gonzalez, W.A. Slawinski, D.S. Wraggc, *Chem. Commun.* **2019**, 55, 1667-1678. d) J. Fan, P. Ning, Y.C. Wang, Z.X. Song, X. Liu, H.M. Wang, J. Wang, L.Y. Wang, Q.L. Zhang, *Chem. Eng. J.* **2019**, 369, 908-919.
- [7] R. Martínez-Franco, M. Moliner, C. Francha, A. Kustov, A. Corma, *Appl. Catal. B* **2012**, 127, 273-280.
- [8] L.M. Ren, L.F. Zhu, C.G. Yang, Y.M. Chen, Q. Sun, H.Y. Zhang, C.J. Li, F. Nawaz, X.J. Meng, F.S. Xiao, *Chem. Commun.* **2011**, 47, 9789-9791.
- [9] L. Zhang, Q.M. Wu, X.J. Meng, U. Müller, M. Feyen, D. Dai, S. Maurer, R.M. Guire, A. Moini, A.N. Parvulescu, W.P. Zhang, C. Shi, T. Yokoi, X.L. Pan, X.H. Bao, H. Gies, B. Marler, Dirk E. De Vos, U. Kolb, F.S. Xiao, *React. Chem. Eng.* **2019**, 4, 975-985.
- [10] a) L.J. Xie, F.D. Liu, L.M. Ren, X.Y. Shi, F.S. Xiao, H. He, *Environ. Sci. Technol.* **2014**, 48, 566-572. b) L.J. Xie, F.D. Liu, X.Y. Shi, F.S. Xiao, H. He, *Appl. Catal. B* **2015**, 179, 202-206.
- [11] U. Deka, I.L. Gonzalez, S.J. Warrender, A.L. Picone, P.A. Wright, B.M. Weckhuysen, A.M. Beale, *Micropor. Mesopor. Mater.* **2013**, 166, 144-152.
- [12] R. Li, P.Q. Wang, S.B. Ma, F.L. Yuan, Z.B. Li, Y.J. Zhu, *Chem. Eng. J.* **2020**, 379, 122376-122377.
- [13] J.X. Liu, F.H. Yu, J. Liu, Y.C. Wei, Q.Y. Sun, *J. Environ. Sci.* **2016**, 48, 45-58.
- [14] a) L.P. Han, M. Gao, J.Y. Hasegawa, S.X. Li, Y.J. Shen, H.R. Li, L.Y. Shi, D.S. Zhang, *Environ. Sci. Technol.* **2019**, 53, 6462-6473. b) R. Yan, S.X. Lin, Y.L. Li, W.M. Liu, Y.Y. Mi, C.J. Tang, L. Wang, P. Wu, H.G. Peng, *J. Hazard. Mater.* **2020**, 396, 122592.
- [15] J.M. Ramallo-López, L.B. Gutierrez, A.G. Bibiloni, F.G. Requejo, E.E. Miró, *Catal. Lett.* **2002**, 82, 131-139.
- [16] B.H. Chen, R.N. Xu, R.D. Zhang, N. Liu, *Environ. Sci. Technol.* **2014**, 23, 13909-13916.
- [17] a) X.M. Guo, D.S. Mao, S. Wang, G.S. Wu, G.Z. Lu, *Catal. Commun.* **2009**, 10, 1661-1664. b) J. Baneshi, M. Haghghi, N. Jodeiri, M. Abdollahifar, H. Ajamein, *Energy Convers. Manage.* **2014**, 87, 928-937.
- [18] a) S. Ali, L.Q. Chen, F.L. Yuan, R. Li, T.R. Zhang, S.H. Bakhtiar, X.S. Leng, X.Y. Niu, Y.J. Zhu, *Appl. Catal. B* **2017**, 210, 223-234. b) S. Ali, L.Q. Chen, Z.B. Li, T.R. Zhang, R. Li, S.H. Bakhtiar, X.S. Leng, F.L. Yuan, X.Y. Niu, Y.J. Zhu, *Appl. Catal. B* **2018**, 236, 25-35. c) S.B. Ma, X.Y. Zhao, Y.S. Li, T.R. Zhang, F.L. Yuan, X.Y. Niu, Y.J. Zhu, *Appl. Catal. B* **2019**, 248, 226-238.
- [19] C.D. Yan, H. Cheng, Z.S. Yuan, S.D. Wang, *Environ. Technol.* **2015**, 36, 169-177.

- [20] a) C. Paolucci, J.R. Di Iorio, F.H. Ribeiro, R. Gounder, W.F. Schneider, *Adv. Catal.* **2016**, *59*, 1-107. b) Y. Mao, Z.Y. Wang, H.F. Wang, P. Hu, *ACS Catal.* **2016**, *11*, 7882-7891. c) A Wolberg, J.F Roth, *J. Catal.* **1969**, *15*, 250-255.
- [21] Y.J. Kim, J.K. Lee, K.M. Min, S.B. Hong, I. Nam, B.K. Cho, *J. Catal.* **2014**, *311*, 447-457.
- [22] M. Zamadics, X.H. Chen, L. Kevan, *J. Phys. Chem.* **1992**, *96*, 2652-2657.
- [23] a) C. Negri, E. Borfecchia, M. Cutini, K.A. Lomachenko, T.V.W. Janssens, G. Berlier, S. Bordiga, *ChemCatChem* **2019**, *11*, 1-12. b) L. Wang, J.R. Gaudet, W. Li, D. Weng, *J. Catal.* **2013**, *306*, 68-77. c) S.A. Bates, A.A. Verma, C. Paolucci, A.A. Parekh, T. Anggara, A. Yezerets, W.F. Schneider, J.T. Miller, W.N. Delgass, F.H. Ribeiro, *J. Catal.* **2014**, *312*, 87-97. d) S. Kieger, G. Delahay, B. Coq, B. Neveu. *J. Catal.* **1999**, *183*, 267-280.
- [24] A. Shishkin, H. Kannisto, P.A. Carlsson, H. Härelind, M. Skoglundh, *Catal. Sci. Technol.* **2014**, *4*, 3917-3926.
- [25] a) S.X. Liu, X.D. Wu, D. Weng, L. Shi. *J. Rare Earths.* **2016**, *34*, 1004-1009. b) J. Wang, D. Fan, T. Yu, J. Wang, T. Hao, X. Hu, M.Q. Shen, W. Li. *J. Catal.* **2015**, *322*, 84-90. c) L. Wang, W. Li, S.J. Schmieg, D. Weng. *J. Catal.* **2015**, *324*, 98-106. d) D. Wang, L. Zhang, J.H. Li, K. Kamasamudram, W.S. Epling. *Catal. Today* **2014**, *231*, 64-74.
- [26] G.Y. Zhou, B.C. Zhong, W.H. Wang, X.J. Guan, B.C. Huang, D.Q. Ye, H.J. Wu, *Catal. Today* **2011**, *175*, 157-163.
- [27] a) D. Barthomeuf, *Zeolites* **1994**, *14*, 394-401. b) X.T. Wang, R. Li, S.H. Bakhtiar, F.L. Yuan, Z.B. Li, Y.J. Zhu, *Catal. Commun.* **2018**, *108*, 64-67.
- [28] R. Li, Z.B. Li, L.Q. Chen, Y.L. Dong, S.B. Ma, F.L. Yuan, Y.J. Zhu, *Catal. Sci. Technol.* **2017**, *7*, 4984-4995.
- [29] F. Gao, E.D. Walter, N.M. Washton, J. Szanyi, C.H.F. Peden, *Appl. Catal. B* **2015**, *162*, 501-512.
- [30] a) L.Q. Chen, R. Li, Z.B. Li, F.L. Yuan, X.Y. Niu, Y.J. Zhu, *Catal. Sci. Technol.* **2017**, *7*, 3243-3257. b) Z.P. Zhang, L.Q. Chen, Z.B. Li, P.Y. Li, F.L. Yuan, X.Y. Niu, Y.J. Zhu, *Catal. Sci. Technol.* **2016**, *6*, 7151-7162. c) L.Q. Chen, X.Y. Niu, Z.B. Li, Y.L. Dong, Z.P. Zhang, F.L. Yuan, Y.J. Zhu, *Catal. Commun.* **2016**, *85*, 48-51.
- [31] a) Z. Liu, S.I. Woo, W.S. Lee, *J. Phys. Chem. B* **2006**, *110*, 26019-26023. b) C. Peng, R. Yan, H.G. Peng, Y.Y. Mi, J. Liang, W.M. Liu, X. Wang, G. Song, P. Wu, F.D. Liu. *J. Hazard. Mater.* **2020**, *385*, 121593-121603. c) Z. Liu, H. Su, J. Li, Y. Li, *Catal. Commun.* **2015**, *65*, 51-54. d) S. Ding, F. Liu, X. Shi, K. Liu, Z. Lian, L. Xie, H. He, *ACS Appl. Mater. Interfaces* **2015**, *7*, 9497-9506.
- [32] Y.Y. Yue, B. Liu, N.G. Lv, T.H. Wang, X.T. Bi, H.B. Zhu, P. Yuan, Z.S. Bai, Q.Y. Cui, X.J. Bao. *ChemCatChem* **2019**, *11*, 4744-4754.

Entry for the Table of Contents



Cu/SAPO-34 with excellent NH₃-SCR performance was synthesized for the first time using cupric citrate as a copper source in a one-step method.